SOILS AND FOUNDATIONS Vol. 45, No. 3, 147–159, June 2005
Japanese Geotechnical Society

CONSTITUTIVE MODEL FOR 1-D CYCLIC SOIL BEHAVIOUR APPLIED TO SEISMIC ANALYSIS OF LAYERED DEPOSITS

NIKOS GEROLYMOS[i] and GEORGE GAZETAS[ii]

ABSTRACT

A phenomenological constitutive model, 'BWGG', is developed for the non-linear one-dimensional ground response analysis of layered sites. The model reproduces the nonlinear hysteretic behaviour of a variety of soils, and possesses considerable flexibility to represent complex patterns of cyclic behaviour such as stiffness decay and loss of strength due to build-up of pore-water pressure, cyclic mobility, and load induced anisotropy. It also has the ability of simultaneously generating realistic modulus and damping versus strain curves, by a simple calibration of only three of its parameters. The model is implemented through an explicit finite-difference algorithm into a computer code which perform integration of the wave equations to obtain the nonlinear response of the soil. The code, 'NL-DYAS', is then applied to study the seismic response of a soft marine normally-consolidated clay. The results are compared with those of widely used codes. Finally, the records of the Port Island array during the Kobe 1995 earthquake, are utilized, and the model is shown to "predict" the observed response with sufficient accuracy.

Key words: cyclic loading, damping, nonlinear ground response, Port Island array, shear modulus, soft clay seismic response, soil model (**IGC**: D7/E8/E13)

INTRODUCTION

Site response analysis is a very important issue in earthquake engineering. It is usually the first step in the calculation of structural response in soil-structure interaction problems. Thus, a substantial effort has been devoted in the last three decades in developing analytical techniques and numerical methods for evaluating the response of soil deposits to strong earthquake motions. The majority of practical methods used for describing nonlinear soil amplification are classified into two categories: (a) frequency domain equivalent linear and (b) time domain nonlinear methods.

Although equivalent linear type of analyses are the most popular, they have certain well-known limitations under strong seismic shaking.

On the other hand, many of the commercially available nonlinear models: (a) are incapable of simultaneously fitting the observed shear modulus degradation and damping curves, usually overestimating hysteretic damping at large strains (if the Masing rule for unloading-reloading is used), and (b) are not versatile in properly modeling the shape of various experimental stress-strain loops for various types of soil behaviour. Clearly, the Masing criterion is handly appropriate for cyclic soil behaviour, as demonstrated in the examples of Fig. 1.

A phenomenological 1-D constitutive model, designated as BWGG model, is developed in this paper for the

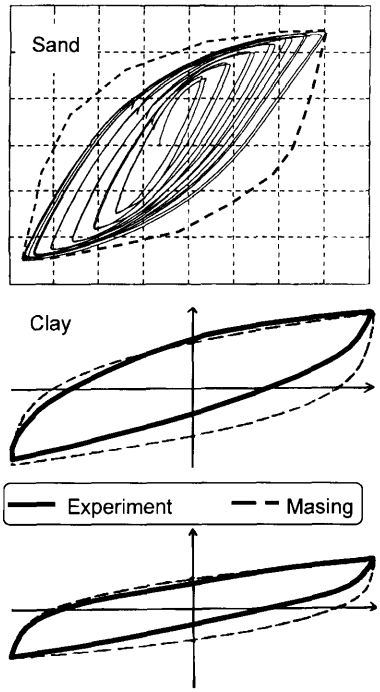

Fig. 1. Shear stress-strain loops for soil elements: Comparison of experimental and theoretical results with Masing rule for unloading-reloading

[i] Post Doctoral Researcher, National Technical University, Athens, Greece.
[ii] Professor of Geotechnical Engineering, ditto (gazetas@compulink.gr).
The manuscript for this paper was received for review on March 24, 2004; approved on March 11, 2005.
Written discussions on this paper should be submitted before January 1, 2006 to the Japanese Geotechnical Society, 4-38-2, Sengoku, Bunkyo-ku, Tokyo 112-0011, Japan. Upon request the closing date may be extended one month.

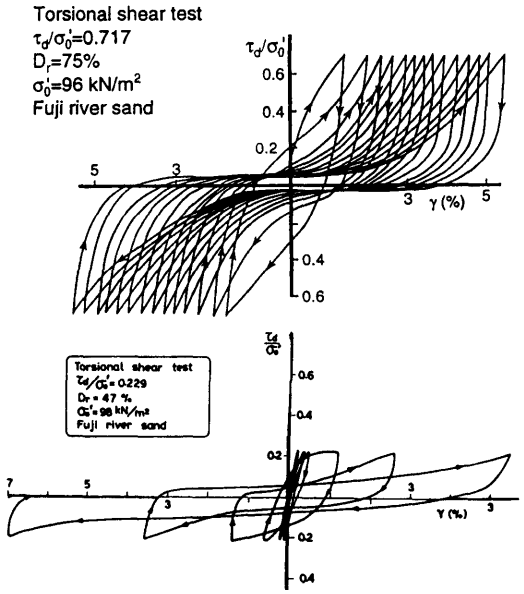

Fig. 2. Typical complicated nonlinear cyclic behavior of soil: (Top) cyclic mobility of dense sand, (Bottom) Liquefaction of sand (Ishihara, 1996)

static and dynamic response of soils. The model avoids the aforementioned disadvantages and is quite versatile, capable of reproducing even some of the most complex nonlinear characteristics of cyclic behaviour, such as the cyclic mobility and liquefaction response depicted in Fig. 2. The model predictions can simultaneously match any experimental modulus decline and damping growth versus shear strain curve by properly adjusting only three of its parameters. The other parameters do not affect the match and can be set equal to their default values, or simply eliminated from the model. Identification and/or complete calibration of the model parameters is beyond the scope of this paper. Nevertheless, a methodology for relating the model parameters to the physical and mechanical soil properties (from in-situ and/or laboratory tests) is briefly discussed. An outline of the model is given below.

THE MODEL: EQUATIONS AND PARAMETERS

The constitutive model proposed here in for modeling the soil simple shear stress-strain relation of a soil element is given by;

$$\tau(t)=aG_{\max}\gamma(t)+(1-a)\tau_y\zeta(t) \tag{1}$$

where τ and γ are the shear stress and strain respectively, $G_{\max}$ is the initial tangent shear modulus, α is a parameter that controls the post yielding shear stiffness, τ_y is the value of shear stress at initiation of yielding in the soil. The parameter $\zeta=\zeta(t)$ is hysteretic dimensionless quantity that controls the nonlinear response of soil, and is governed by the following differential equation;

$$\frac{d\zeta}{dt}=\frac{1}{\gamma_y}\left(A\frac{d\gamma}{dt}-b\frac{d\gamma}{dt}|\zeta|^n-g\left|\frac{d\gamma}{dt}\right||\zeta|^{n-1}\zeta\right) \tag{2}$$

in which A, b, g and n are dimensionless quantities which control the shape of the stress-strain loop; γ_y is the value of shear strain at "initiation of yielding" in the soil. The model of (1) and (2) was originally proposed by Bouc (1971) and subsequently extended by Wen (1976) and used in random vibration studies of inelastic systems. The expressions given by (1) and (2) have been previously used from Pires (1989) and Loh et al. (1995) for probabilistic analysis of the seismic response of multi-layered soil deposits.

By differentiating Eq. (1) with respect to the shear strain γ, one obtains;

$$\frac{d\tau}{d\gamma}=\alpha G_{\max}+(1-\alpha)\tau_y\frac{d\zeta}{d\gamma} \tag{3}$$

where

$$\frac{d\zeta}{d\gamma}=\frac{1}{\gamma_y}\left\{A-|\zeta|^n\left[b+g\,\mathrm{sign}\left(\frac{d\gamma}{dt}\zeta\right)\right]\right\} \tag{4}$$

In monotonic loading conditions Eq. (2) collapses to;

$$\frac{d\zeta}{d\mu}=A-(b+g)\zeta^n \tag{5}$$

where

$$\mu=\frac{\gamma}{\gamma_y} \tag{6}$$

is the strain ductility that the soil element experiences during loading. It can be easily shown that when γ tends to 0, Eq. (6) reduces to;

$$\frac{d\zeta}{d\mu}=A \tag{7}$$

Substituting Eq. (7) to Eq. (3) and setting $\alpha=0$ yields

$$\frac{d\tau}{d\gamma}=\frac{\tau_y}{\gamma_y}A \tag{8}$$

When $A=1$, $G_{\max}(=\tau_y/\gamma_y)$ becomes the small-amplitude shear modulus, while α becomes the ratio of the post-to pre-yielding stiffness.

From Eq. (1) it is obvious that the maximum value of the shear stress, $\tau_{\max}$, is reached when γ and ζ take their maximum value. For monotonic loading the maximum value of ζ is obtained by setting $d\zeta/d\gamma=0$, and by virtue of Eq. (3) this maximum takes the value;

$$\zeta_{\max}=\left(\frac{A}{b+g}\right)^{1/n} \tag{9}$$

Substituting Eq. (9) to Eq. (1) and setting $\tau=\tau_{\max}$, $\alpha=0$, and $\zeta=\zeta_{\max}$ one obtains;

$$\tau_{\max}=\tau_y\left(\frac{A}{b+g}\right)^{1/n} \tag{10}$$

Note that the maximum shear stress becomes equal to τ_y when

$$A=b+g \tag{11}$$

In undrained loading conditions, τ_y is equal to the undrained shear strength S_u.

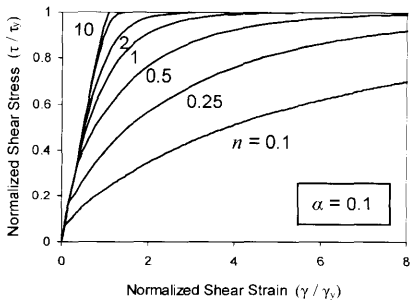

Fig. 3. Normalized stress-strain curves to monotonic loading for selected values of parameter n, computed from the proposed model for soils

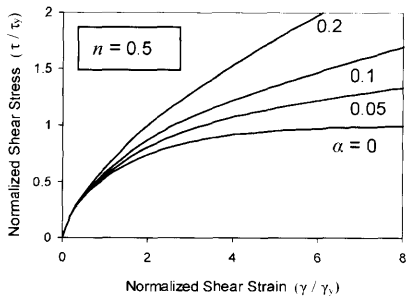

Fig. 4. Normalized stress-strain curves to monotonic loading for selected values of post-yielding parameter α and $n=0.5$, computed from the proposed model for soils

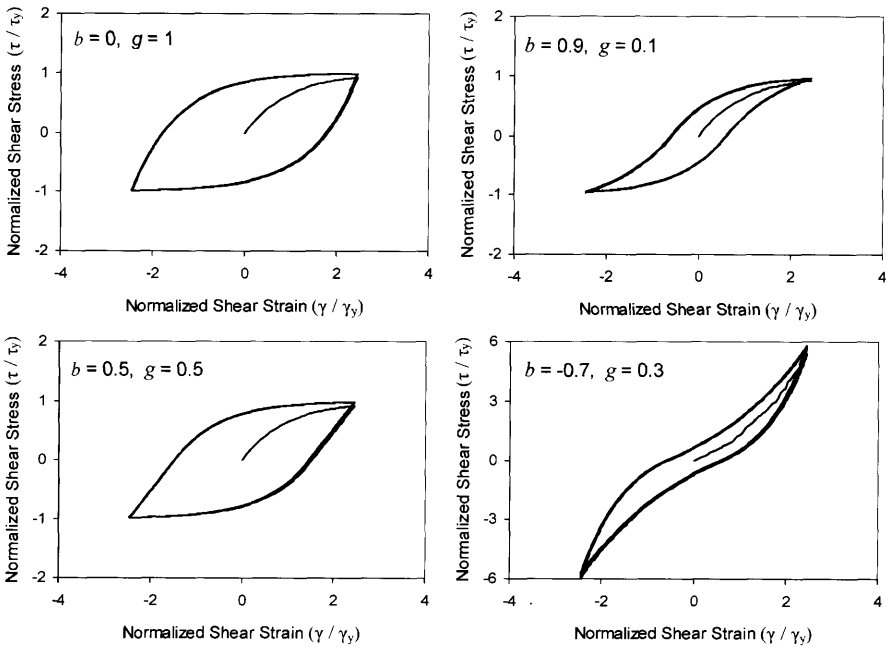

Fig. 5. Hysteretic normalized stress-strain loops for different values of b and g, $n=1$: The Masing criterion for unloading-reloading is obtained for $b=0.5$, $g=0.5$

Monotonic Loading Curve

The parameter n governs the sharpness of the transition from the linear to nonlinear range during initial virgin loading. Its range of values is between 0 and ∞, with the $\tau-\gamma$ curve approaching bilinear behaviour as n approaches ∞. However elastic-perfectly plastic behaviour is practically achieved when n takes values greater than 10. The effect of parameter n on the monotonic loading curve is portrayed in Fig. 3. As the values of n decrease plastic straining appears even at low loading levels. Monotonic loading curves for different values of the post yielding parameter α and for constant value of n are also presented in Fig. 4.

Loading-Unloading-Reloading Rule

Parameters b and g control the shape of the unloading-reloading curve. As is shown in Fig. 5 there are four basic hysteretic shapes, which depend on the relation between b and g. As b tends to 1 and by virtue of $b+g=1$, the reversal stiffness tends to 0. For the special case $b=1$ and $g=0$, the stress-strain loop collapses to the monotonic loading curve (nonlinear elastic behaviour). On the contrary as g reaches 1 under the condition of $b+g=1$, the reversal stiffness becomes greater than the initial stiffness (at virgin loading). Finally when $b=g=0.5$ the reversal stiffness equals the initial stiffness and the Masing criterion for loading-unloading-reloading arises.

Stiffness and Strength Degradation with Cyclic Loading

The model is capable of reproducing stiffness and strength degrading behaviour. Stiffness decay is achieved by introducing the parameter η in Eq. (2), giving;

$$\frac{d\zeta}{dt}=\eta\frac{1}{\gamma_y}\left(A\frac{d\gamma}{dt}-b\frac{d\gamma}{dt}|\zeta|^n-g\left|\frac{d\gamma}{dt}\right||\zeta|^{n-1}\zeta\right) \qquad (12)$$

Prescribing η to be an increasing function of time will induce stiffness decay. η can be expressed as a function of the dissipated hysteretic energy and/or the cumulative strain ductility. Note that decreasing η is equivalent to reducing A, b and g in proportion. The flexibility of

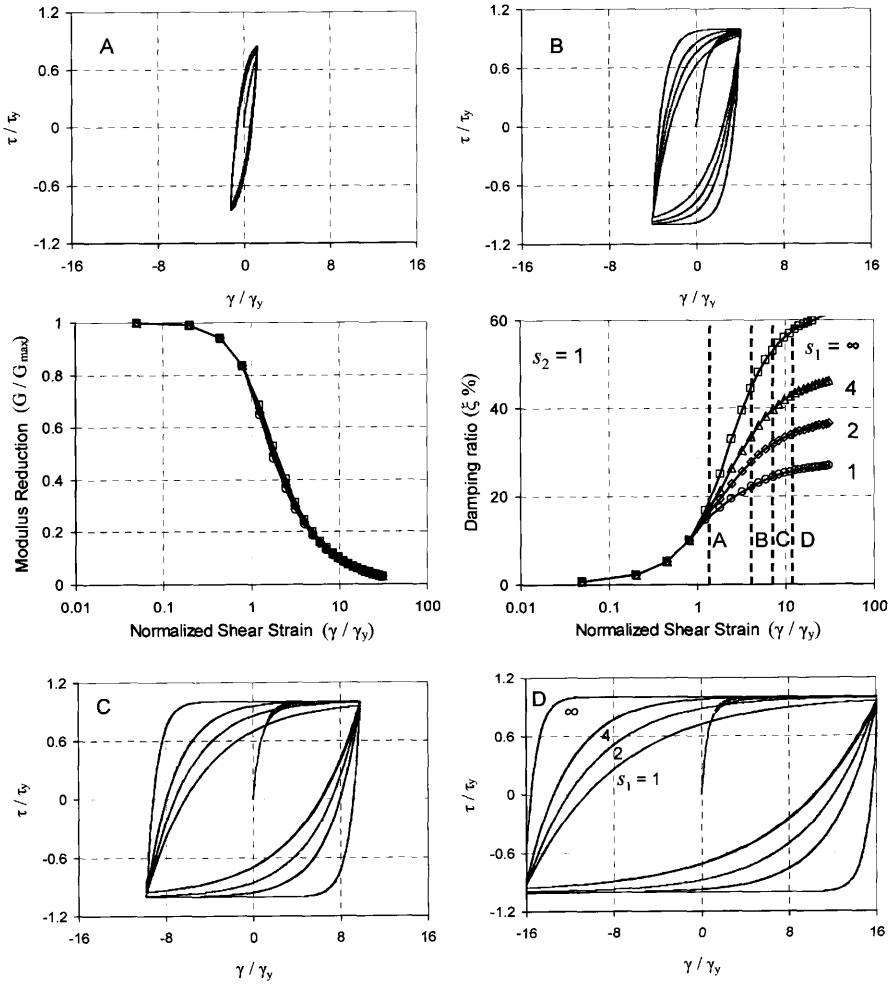

Fig. 6. Stress-strain loops computed by BWGG model for soils, for selected values of s_1 together with the corresponding shear modulus and damping curves ($b=0$, $g=1$ and $n=1$)

the model in adjusting secant modulus reduction and damping independently is extended by expressing η in the following ductility-based form.

$$\eta=\frac{s_1+a(\mu_r+1)+s_2}{s_1+\mu_r}, \quad \text{for} \quad \mu_r>s_2 \tag{13}$$

and

$$\eta=1, \quad \text{for} \quad \mu_r<s_2 \tag{14}$$

where μ_r is a reference strain ductility defined in terms of the shear strain at the most current stress reversal, and the maximum attained shear strain before the start of the current unloading or reloading cycle. The parameter s_1 controls the reversal stiffness while the parameter s_2 is a characteristic value of strain ductility, γ/γ_y, beyond of which the stiffness degradation initiates.

Typical stress-strain loops for selected values of s_1 are depicted in Fig. 6 together with the corresponding shear modulus and damping versus strain curves. Increasing values of s_1 leads to more rapid increase of damping for strain amplitudes bigger than $s_2\gamma_y$. It is worthy of note that the greater the strain amplitude the less stiff is the response at load reversal while the secant stiffness remains constant. It is also shown from Fig. 6 that while the damping curves cover a very broad range, all the shear modulus curves fall within a very narrow zone, revealing the independence between the two group of curves, primarily thanks to the key parameter s_1. Note that only when s_1 tends to infinity, the damping tends to (the unrealistically high) $2/\pi$ at large strains.

The proposed model is also versatile in simulating strength degradation with cyclic loading. This can be achieved in two different ways: (a) By making parameters b and g increasing functions of hysteretic energy and/or of cumulative strain ductility, while fulfilling the condition of equal reduction of b and g; (b) both strength and stiffness degradation can be affected by incorporating the parameter r in Eq. (1) giving;

$$\tau(t)=\lfloor aG_{max}\gamma(t)+(1-a)\tau_y\zeta(t)\rfloor\ (1-r) \tag{15}$$

Increasing r is equivalent to reducing parameter A without affecting b and g. Parameter r can be prescribed as an increasing function of dissipated energy. The dissipated energy has been widely used by many researchers as a measure of cyclic strength degradation and subsequently of liquefaction resistance of saturated grained soils. Relationships between excess pore pressure and dissipated energy have been established from ex-

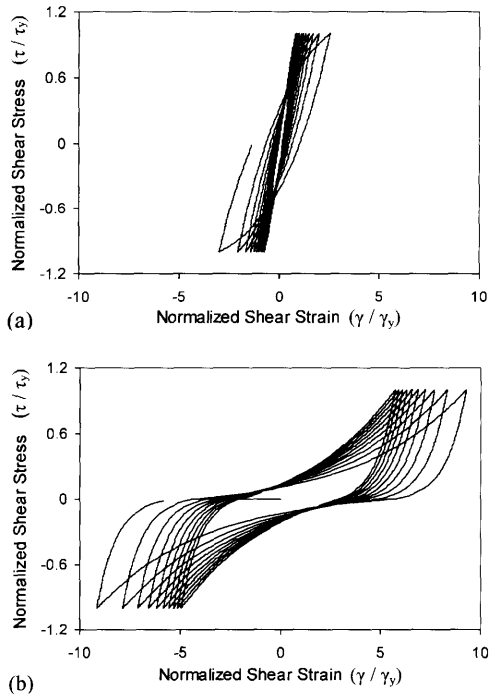

Fig. 7. Normalized stress-strain loops for soil elements experiencing stiffness and strength degradation with cyclic loading, computed by BWGG model for soils: The loops are characteristic of sand experiencing pore-water pressure build up: (a) before the initiation of cyclic mobility and (b) during the phase of cyclic mobility

perimental data. By fitting these data, r can be expressed as;

$$r=\frac{\Delta u}{\sigma'_{v0}}=aW_N^{\beta} \tag{16}$$

where Δu is the incremental pore pressure build up, σ'_{v0} is the initial vertical effective stress, W_N is a dimensionless energy term (Law et al., 1990) and a and β are determined from laboratory tests. Parameter r can be adapted to incorporate any pore pressure model (e.g. Ishihara and Towhata, 1980; Finn et al., 1977). Figure 7 depicts stress-strain loops for soil elements experiencing stiffness and strength degradation with cyclic loading, computed with the proposed model for soils. The loop of Fig. 7(a) corresponds to values of b and g equal to 0.5, whereas that of Fig. 7(b) to $b=-0.6$ and $g=0.4$. The stress-strain loops of Figs. 7(a) and 7(b) are characteristic of a sand behaviour experiencing pore-water pressure build up, just a little before the initiation and during the cyclic mobility, respectively. To simulate the transition between these two different phases of soil behaviour would require calibration against laboratory data of parameter r, or alternatively of parameters b and g, in time domain. For example r should be an increasing function of time before the initiation of cyclic mobility, experiencing fluctuations with time (for simulating the strain hardening response). Since identification and complete calibration of the model parameters is beyond the scope of this paper, the stress-strain loops in Fig. 7 shall be considered purely as a demonstration of the potential capabilities of the proposed model for soil.

To further extend the capabilities of the model in simulating the cyclic response of soil elements undergoing cyclic mobility, Eq. (12) is modified by introducing the term;

$$P(\zeta)=\frac{1}{L_s}\exp\left[\left(\frac{\zeta-\zeta_2}{\zeta_1}\right)^2\right] \tag{17}$$

leading to the following differential equation

$$\frac{d\zeta}{dt}=\eta\frac{1}{\gamma_y}\frac{A\dfrac{d\gamma}{dt}-b\dfrac{d\gamma}{dt}|\zeta|^n-g\left|\dfrac{d\gamma}{dt}\right||\zeta|^{n-1}\zeta}{1+\left[A-b|\zeta|^n-g\,\mathrm{sign}\left(\dfrac{d\gamma}{dt}\right)|\zeta|^{n-1}\zeta\right]\left\{L_s\exp\left[-\left(\dfrac{\zeta-\zeta_2}{\zeta_1}\right)^2\right]\right\}} \tag{18}$$

L_s and ζ_1 are dimensionless parameters which control the narrowing of the hysteretic loop around the center of the stress-strain axis. ζ_2 is a constant that controls the shift of the backbone curve on the ζ axis. The influence of parameter L_s on the shape of stress-strain loop is illustrated in Fig. 8. Notice that the larger the L_s, the more pronounced the narrowing of the hysteretic loop around the center of stress-strain axis.

The mechanical analog of Eq. (18) is that of two springs placed in parallel. The first spring "constant" represents the tangent shear stiffness of the soil and is given by;

$$K_s=\frac{d\zeta^*}{d\gamma} \tag{19}$$

with ζ^* governed by Eq. (12). The modulus of the second spring, $P(\zeta)$, stands for improving the modelling of dilative soil behaviour. To this end, Eq. (18) can be rewritten in the equivalent form;

$$\frac{d\zeta}{d\gamma}=\frac{\dfrac{d\zeta^*}{d\gamma}P(\zeta)}{\dfrac{d\zeta^*}{d\gamma}+P(\zeta)} \tag{20}$$

Figure 9 depicts a typical stress-strain loop computed with the use of Eq. (18), corresponding to the cyclic behaviour of a dense sand undergoing cyclic mobility.

Asymmetric Response with Loading Direction

Finally, the non-symmetric cyclic response of soil with

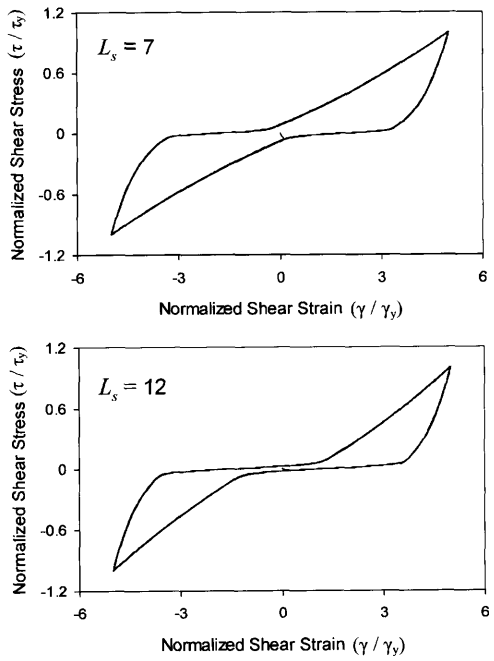

Fig. 8. Normalized stress-strain loops for selected values of parameter L_s, computed by BWGG model for soils ($n=1$, $b=-0.6$, $g=0.4$)

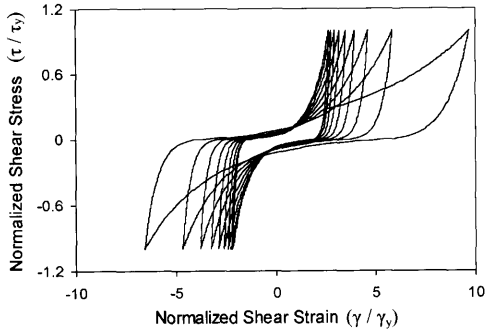

Fig. 9. Typical stress-strain loop computed by BWGG model for soils, corresponding to the cyclic behavior of a dense sand undergoing cyclic mobility

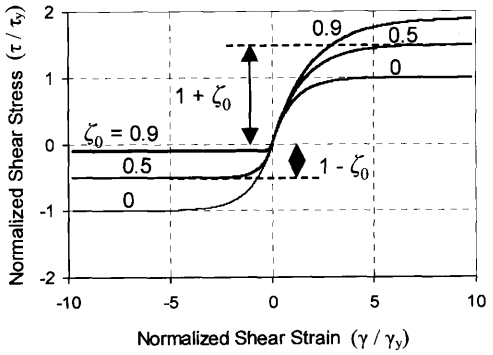

Fig. 10. Normalized stress-strain curves to monotonic loading for selected values of parameter ζ_0, computed by BWGG model for soils

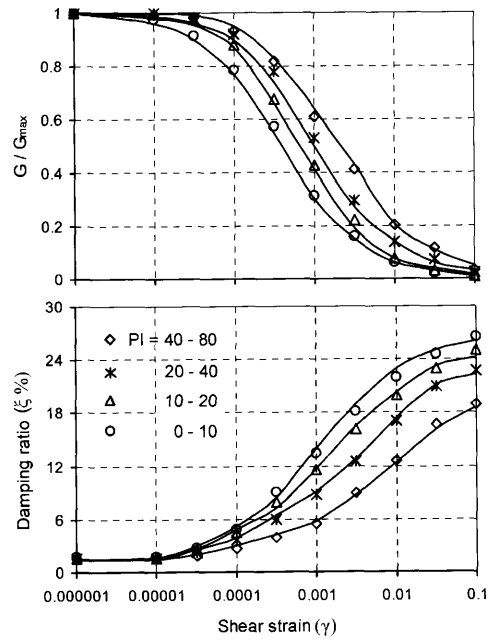

Fig. 11. BWGG Model prediction of Vucetic and Dobry experimental curves

respect to loading direction can be modeled by replacing ζ in the numerator at the right-hand side of Eq. (2), with

$$\zeta_r = \frac{\zeta}{1+\zeta_0 \,\mathrm{sign}\left(\frac{d\zeta}{dt}\right)} \tag{21}$$

where ζ_0 is a constant that controls the shift of the backbone curve on ζ axis. Figure 10 illustrates the stress-strain monotonic loading curves computed for selected values of ζ_0.

SHEAR MODULUS REDUCTION AND DAMPING CURVES

One of the major advantage of the proposed model for soils is its ability to independently match the observed shear modulus degradation and damping for any given soil, by simply calibrating only three of its parameters, n, s_1 and s_2 (defined in the previous section). An optimization procedure has also been developed to evaluate the three parameters to fit the observed behaviour, the presentation of which however is beyond the scope of this article. As can be seen from the graphs in Fig. 11 the model simulates the secant modulus and damping, in accord with the measurements in Vucetic and Dobry (1989).

DISCUSSION ON THE MODEL PARAMETERS

The proposed model is a system of equations capable of reproducing the cyclic soil behaviour, when its parameters are appropriately chosen. However, it does not include any physically motivated stress-strain relation. This means that identification and calibration of the model parameters is a compulsory task. This could be

done by utilizing data from:

- laboratory tests such as cyclic triaxial and cyclic simple shear
- in situ tests such as the standard penetration (SPT) and the crosshole
- recorded free-field response
- centrifuge or large shaking table soil response.

To this end, nonlinear optimization techniques could be used (such as time domain least square procedure, and dynamic neural networks). For details about a comprehensive method for the identification of the Bouc-Wen model parameters, the reader is referred to the work of Sues, Mau, and Wen (1988). The development of a complete methodology for the identification of the model parameters is not in the scope of this paper. Nevertheless, it is very important to mention that the model has a powerful advantage: the number of the necessary parameters for analysis purposes can be adapted to the amount of the available geotechnical data. The other parameters can be set equal to their default values or simply eliminated from the model. The lesser the in situ and/or laboratory data, the fewer the number of the necessary-for the analysis parameters, but of course, the larger the uncertainty in the model.

For example, supposing we have to conduct a site response analysis and the only available information about the soil are the shear wave velocity profile V_s, the soil classification, and the Atterberg limits, the following steps shall be carried out for calibrating the model parameters: (i) Calculate the small-amplitude shear modulus G_{max}. (ii) Correlate the small-amplitude shear modulus with the undrained shear strength (for clay) and/or the relative density with the internal friction angle (for sand). (iii) Set the yield shear stress τ_y equal to the shear strength of the soil. (iv) Calculate the yield shear strain $\gamma_y = \tau_y / G_{max}$. (v) Choose the appropriate shear modulus reduction and damping curves from the literature, according to soil type, plasticity index, and effective confining pressure. (vi) Calibrate the parameters n, s_1, and s_2 for the calculated shear modulus and damping curves to match the experiment. The other parameters of the model are not needed since the geotechnical data are not adequate for calibrating them. Therefore, they must be set equal to their default values or even be eliminated from the model. That is: set $b = 0.5$, and eliminate α, r, L_s, ζ_1, ζ_2, and ζ_0.

On the other hand, supposing that (except from the aforementioned data) we have also in our disposal results from cyclic undrained triaxial tests, then the proposed methodology is further extended to incorporate additional parameters to account for the effect of the pore-water pressure build up on the stress-strain loop. As we have already mentioned in a previous section, this can be achieved in two different ways: (i) by expressing parameters b and g as a function of hysteretic energy and/or of cumulative strain without affecting r, and (ii) by prescribing r as a function of the effective confining pressure, without affecting b and g. Reevaluation of the strength parameter τ_y could also be done, by using the results of the triaxial tests which are more accurate than those from the empirical correlations.

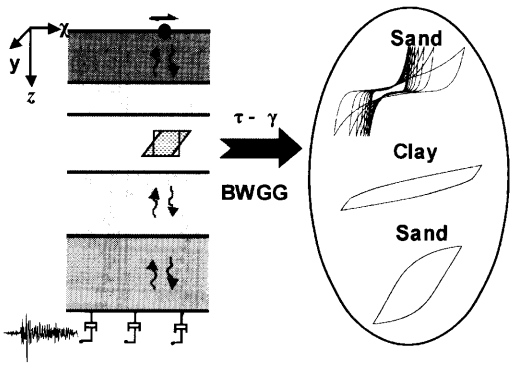

Fig. 12. Schematic illustration of the BWGG model for nonlinear one-dimensional ground response analysis of layered sites

A question then arises about the role of the 'pinching' parameters L_s, ζ_1, and ζ_2, and the parameter for asymmetric response with loading direction ζ_0, in simulating the shape of a stress-strain loop. These parameters aim at further improving the capability of the model in matching the measured soil behaviour. They are simply curve-fitting parameters, not associated with the soil properties. Besides, it is well-known that the larger the number of parameters in a soil model, the more flexible it becomes in reproducing the observed soil behaviour.

NUMERICAL MODELING OF ONE-DIMENSIONAL WAVE PROPAGATION

The problem studied herein is that of a layered soil profile subjected to seismic excitation. The one-dimensional vertical shear wave propagation through a continuum is described by the differential equation;

$$\rho \frac{\partial^2 u}{\partial t^2} = \frac{\partial \tau}{\partial z} + c \frac{\partial^3 u}{\partial z^2 \partial t} \tag{22}$$

where z is depth from surface, t is time, u is soil displacement, τ is soil shear stress, ρ is soil density, and c is viscoelastic constant. The boundary conditions at the base (rock outcrop motion) and at the top of the soil profile are, respectively;

$$\tau(0, t) + c \frac{\partial^2 u}{\partial z \partial t} = \rho_r V_r \left[\frac{du(0, t))}{dt} - \frac{du_g(t)}{dt} \right] \tag{23}$$

and

$$\frac{du(H, t)}{dz} = 0 \tag{24}$$

where ρ_r and V_r the density and shear wave velocity respectively of the rock, H is the thickness of the soil deposit, and $u_g = u_g(t)$ the displacement history of the input "rock outcrop" motion.

The proposed model is schematically illustrated in Fig. 12. An explicit finite difference technique is used for the solution of the field Eq. (22) which is coupled with the constitutive Eqs. (15) and (18), and the boundary

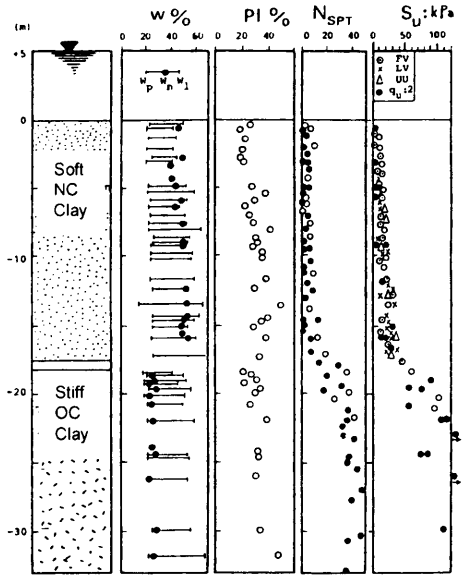

Fig. 13. The soil profile and available geotechnical for our example: The shear modulus is taken as proportional to S_u and hence proportional to depth

Eqs. (23) and (24). We have incorporated the BWGG model into a computer algorithm named NL-DYAS for the nonlinear one-dimensional ground response analysis of layered sites (Gerolymos, 2002).

NONLINEAR SEISMIC RESPONSE ANALYSIS OF A LAYERED SITE-COMPARISON WITH OTHER METHODS

For a first evaluation of the model, a soil amplification analysis is performed for a comparison with codes widely used in geotechnical engineering. More specifically, the seismic response of a representative soil profile of the St. Stefanos bay area in Halkida (Greece), is studied. The soil profile and available geotechnical data are given in Fig. 13. The profile consists of about 18 m soft normally consolidated clay which is underlain by about 16 m thick of stiff overconsolidated clay over-weathered limestone encountered at -34 m. The profile is analysed using: (a) the outlined BWGG model implemented in NL-DYAS, (b) the equivalent linear method (SHAKE-Schnabel et al., 1972), and (c) the hyperbolic model in conjunction with an expanded Masing rule for unloading and reloading (DESRA-Lee et al., 1978). The idealized shear wave velocity and undrained shear strength used in our analyses is illustrated in Fig. 14. The calibration of the model parameters was based on the optimum fit of the published experimental shear modulus reduction and damping curves, using the methodology developed in a previous section. Specifically, the values of the parameters used in the analysis are: $n=0.6$, $b=0.5$, $s_1=1.2$, and $s_2=0.25$. The other parameters are eliminated from the model. The profile was subjected to a seismic accelerogram (Sepolia record) from the Athens 1999 Earthquake ($M_s=5.9$, $\Delta=10$ km), which had a peak ground acceleration of 0.42 g, in order to examine the modeling ability at large

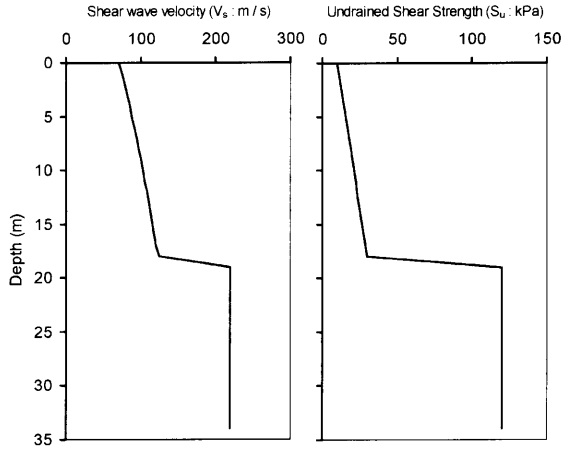

Fig. 14. The idealized shear wave velocity and undrained shear strength profiles used in our analyses

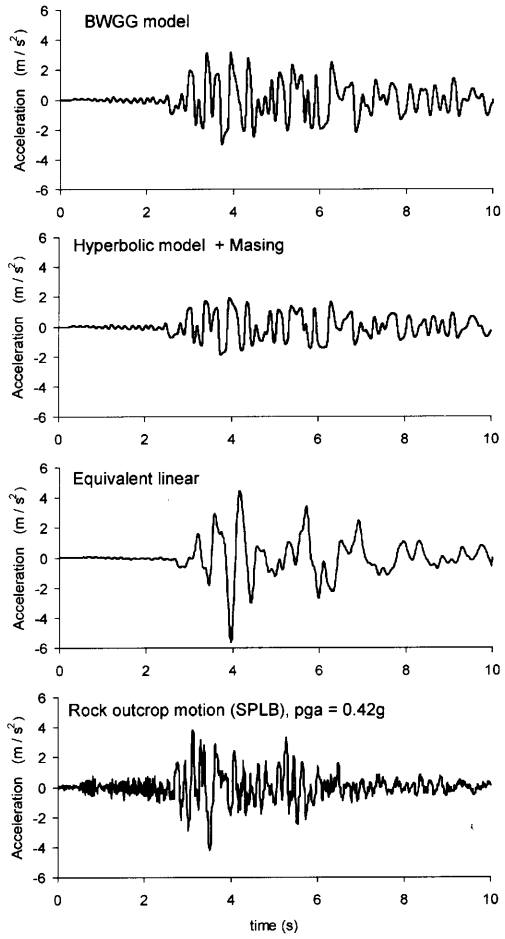

Fig. 15. The seismic excitation (Sepolia Record, Athens 1999 earthquake) and acceleration time histories at the ground surface computed with three models for the soil profile of Fig. 14

strains. The results of the analyses for the three soil models are compared in Figs. 15–17. The following remarks are worthy of note:

(a) Whereas the equivalent-linear SHAKE analysis predicts pga = 0.58 g, the nonlinear inelastic analyses (NL-DYAS and DESRA) predict 0.32 g and 0.19 g,

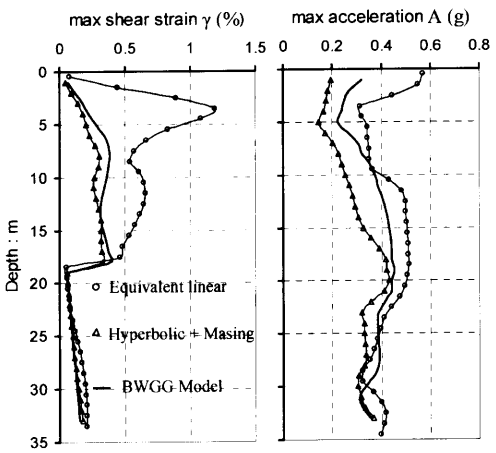

Fig. 16. Comparison of maximum shear strains and acceleration distributions computed with the three models for the soil profile of our example

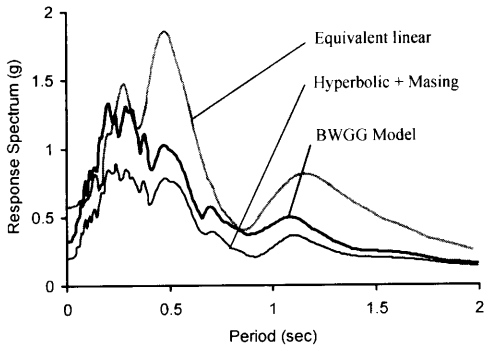

Fig. 17. Comparison of acceleration response spectra at ground surface computed with the three models for the soil profile of our example

respectively. This reveals that significant errors could emerge when ignoring the true nature of soil nonlinearity.

(b) The hyperbolic model in conjunction with the Masing rule for unloading-reloading imposes a systematic cutting-off the acceleration peaks. The value of the limiting acceleration, 0.19 g , is a function of both the minimum value of S_u at the surface, $S_u(0)$ and the rate of increase of S_u with depth, dS_u/dz. Of course, no such cutting-off exists in the equivalent linear analysis. On the other hand, the BWGG model restrains the acceleration peaks but without completely cutting them off at a constant value. This intermediate behaviour stems partially from the hardering parameter α. It is believed to be in closer agreement with reality.

(c) A substantial difference exists between the shear strain amplitudes computed with the equivalent linear and the two nonlinear methods. At a depth of about 4 m we compute max $\gamma \approx 1.2\%$ with the SHAKE analysis, while max $\gamma \approx 0.25\%$ according to both DESRA and NL-DYAS. It is precisely this large strain value which in SHAKE leads to the doubling of acceleration: from the value max $A \approx 0.30$ g at $z = 4$ m to the value max $A \approx 0.58$ g at $z = 0$ m—a phenomenon reminiscent of the "whip-lash" effect in flexible systems vibrating in a higher mode (Travasarou and Gazetas, 2003).

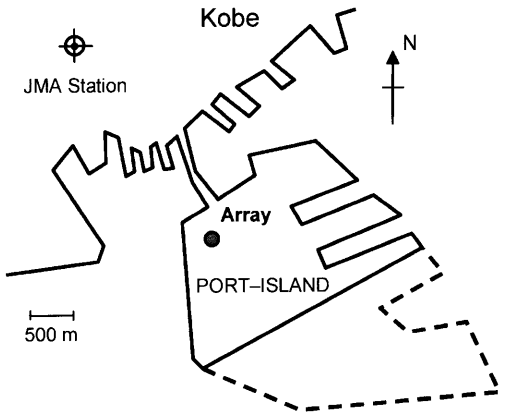

Fig. 18. Location of the Port Island array

(d) The frequency content of the surface motions, as seen in the acceleration histories, and their response spectra, is rather sensitive to the soil model used in the analysis. Indeed, the equivalent linear analysis filters substantially the high-frequency components of the excitation, such as those in the time internal 4.5–6.0 sec. This happens for two reasons: *(i)* throughout shaking the material damping ratio in the equivalent-linear analysis remains constantly 18% near the ground surface, and *(ii)* also throughout shaking, the effective stiffness remains constantly low at about 20% of the original G_{max} (at $\gamma_{eff} \approx (2/3) \max \gamma \approx 0.8\%$). Apparently spuriously high damping and low stiffness are the result of the preceding highest amplitude of acceleration at $t \approx 4$ sec, which controls the equivalent linear response. The two effects combined give the observed artificial filtering of the high frequency components associated with small amplitude oscillations. In contrast, the hyperbolic-Masing model filters (perhaps excessively) the low-frequency high-amplitude components, due to the aforementioned cutting-off process. BWGG captures more accurately than the above two models both the high and low amplitude periods of shaking, as will be further proven in the following case history.

SEISMIC RESPONSE OF PORT ISLAND IN THE 1995 KOBE EARTHQUAKE: ANALYSIS AND RECORDS

The BWGG model for soils is further used to analyse the seismic response in Kobe's Port Island at the in-depth seismographic array where surface and downhole instruments (at −16 m, −32 m, and −82 m) have recorded the shaking during the Great Hanshin (Kobe) Earthquake (1995). These records are the benchmark against which any new method must be tested.

Site Conditions and Seismic Records

A downhole accelerometer array was situated at the north-west corner of Port Island (Fig. 18). The array consisted of triaxial accelerometers located at the three

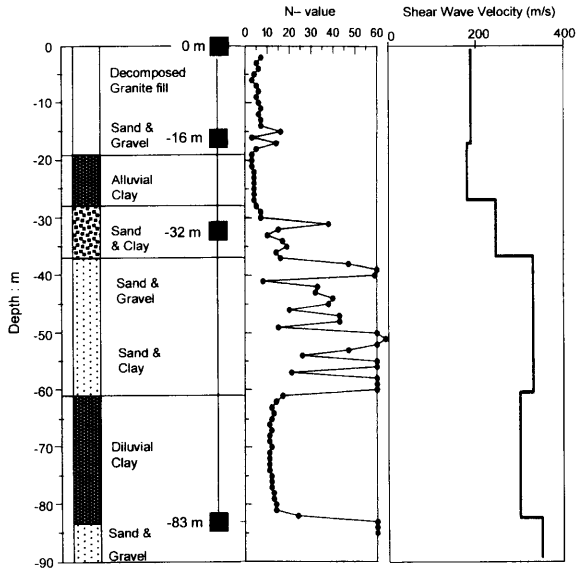

Fig. 19. Soil Profile, SPT and shear wave velocities distributions at the Port Island site (after Iwasaki, 1995)

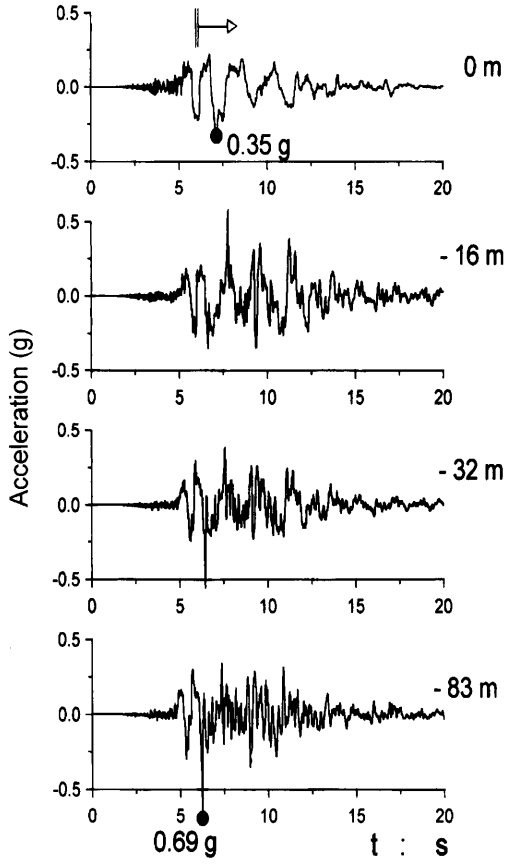

Fig. 20. N44W accelerations at ground surface and downhole stations (at 16 m, 32 m and 83 m depths, after Iwasaki, 1995)

mentioned depths and at the surface. Due to a detailed geotechnical investigation of the array site, performed before and after the earthquake, the soil profile is known with sufficient accuracy (as is summarized in Fig. 19). The subsurface layer down to a depth of 19 m consists of the granular fill layer, underlain by an alluvial clay layer between 19 m and 27 m depth, followed by sandy-gravelly strata interlayered with clay down to 61 m depth. Below is a diluvial clay layer from 61 m to 82 m depth, and a gravelly sand layer starting at 82 m depth. The water table is located at 4 m depth approximately. Figure 19 (after Iwasaki, 1995) shows the soil profile together with the Standard Penetration Test (SPT) N values and the shear wave velocity distributions. The low SPT values in the granular fill justify the high excess pore pressures/liquefaction that took place in this layer. The N44W components of the recorded downhole accelerations are presented in Fig. 20 (after Iwasaki, 1995).

Previous Numerical Simulations of the Seismic Response of the Site

According to Yamazaki et al. (1995) who computed the seismic response of the site, liquefaction may have had occurred in more than one layer at different times. First at 27 m to 33 m depth, and then in the loose layer at 10 m to 16 m depth. Elgamal et al. (1995) who also carried out soil amplification analysis of the site, showed that below 32 m depth the soil response was essentially linear with no appreciable reduction in stiffness. On the other hand, at shallow depths a reduction in soil stiffness with a slight shear strain hardening at elevation 24 m, and an abrupt sharp loss of stiffness accompanied by reduction of yield strength at 8 m depth, was predicted.

Site Response Analysis

The profile is analysed using: (a) the BWGG model implemented in NL-DYAS, and (b) the hyperbolic model in conjunction with Masing rule for unloading and reloading (DESRA). Although the proposed model is capable of reproducing cyclic liquefaction response, the calibration of the model parameters was based exclusively on the best fit to the experimental shear modulus and damping curves (Kokusho et al., 1996). Stiffness and strength degradation due to pore-pressure rise was not taken into account. Specifically, the values of the parameters used in the analysis are: For the sand and gravel layers, $n=1.2$, $b=0.5$, $s_1=1.1$, $s_2=0.15$, and $\alpha=0.035$. For the clay layers, $n=0.6$, $b=0.5$, $s_1=1.2$, $s_2=0.25$, and $\alpha=0.035$. The other parameters are simply eliminated from the model. The N44W earthquake record at 83 m depth (Fig. 20) was used as input excitation of the soil profile.

Figures 21 and 22 show comparison between recorded and calculated motions at the ground surface for both the BWGG model (NL-DYAS) and the hyperbolic plus Masing (DESRA). Stress-strain loops computed by the two models at depths of 20 m and 32 m respectively are also compared in Fig. 23.

The agreement for the proposed model with the record appears to be excellent in the region of the first 6 sec (i.e., before liquefaction has apparently occurred). This is also reflected in the comparison of Fig. 24 in which the predicted spectrum values corresponding to the first 6 sec of the seismic motion, match the recorded spectrum with very good accuracy. As expected, the post-liquefaction

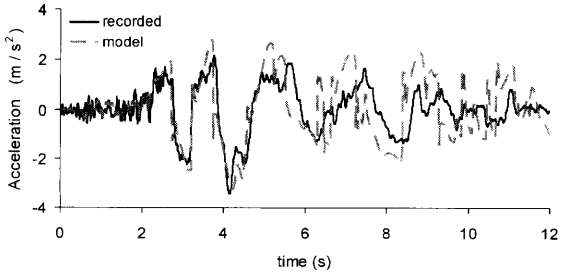

Fig. 21. Comparisons between the recorded accelerogram and the acceleration history computed with BWGG model (dotted line) for the surface

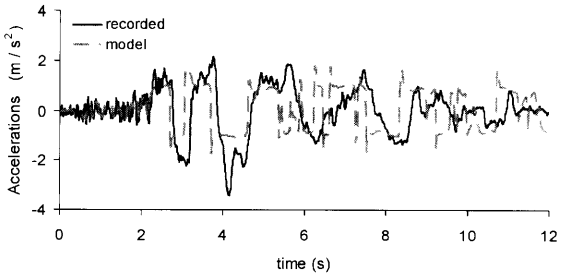

Fig. 22. Comparisons between the recorded accelerogram and the acceleration history computed with hyperbolic model (dotted line) for the surface

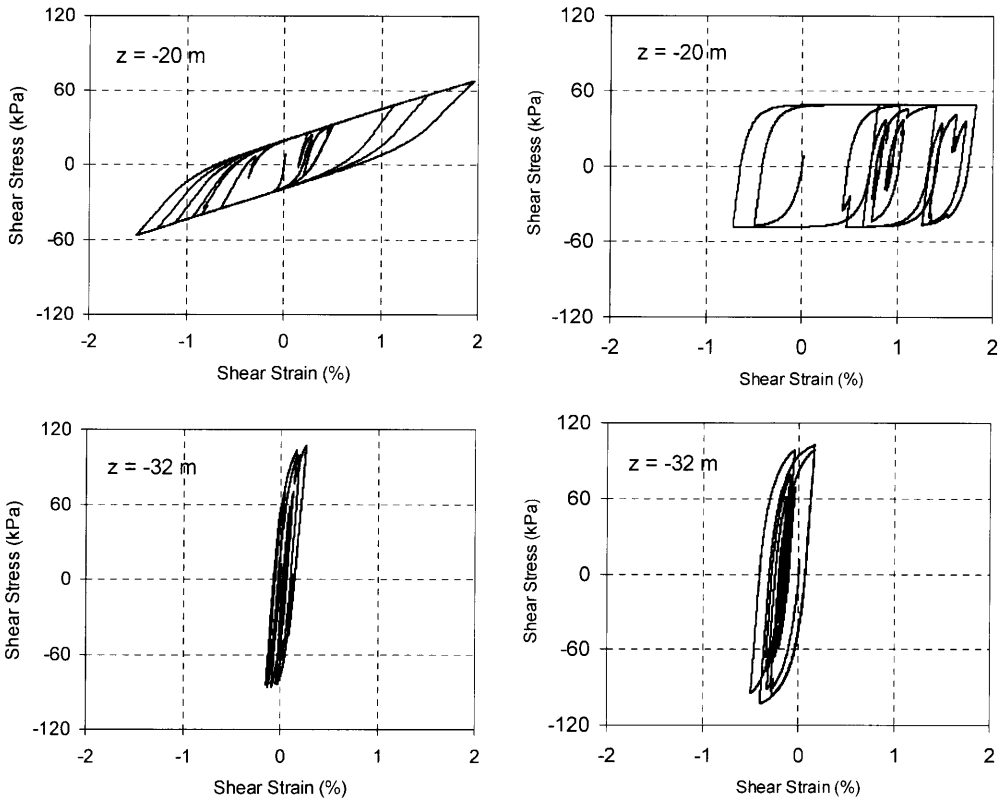

Fig. 23. Shear stress-strain loops computed by the two models at selected depths: (Left) The BWGG model, (Right) The hyperbolic model with the Masing rule for unloading-reloading

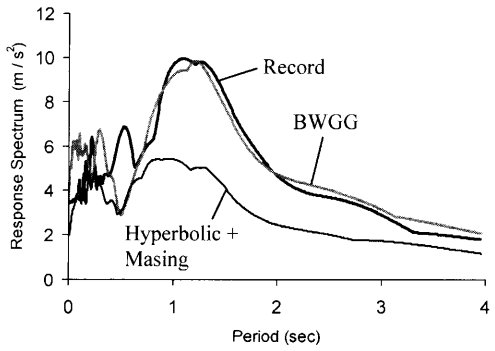

Fig. 24. Comparison between the response spectrum of the first 6 sec of the recorded accelerogram at the ground surface, and the spectra of the first 6 sec of motion computed with the two nonlinear models (BWGG and hyperbolic + Masing)

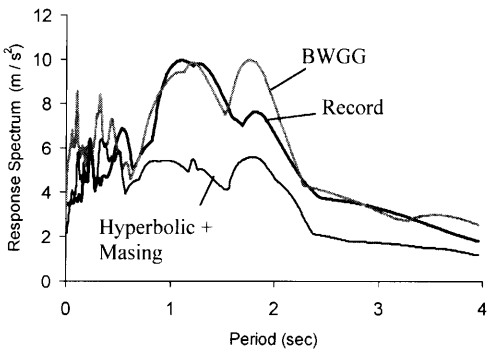

Fig. 25. Comparison between the response spectrum of the complete time history of the recorded accelerogram at the ground surface, and the spectra of the complete time history computed with the two nonlinear models (BWGG and hyperbolic + Masing)

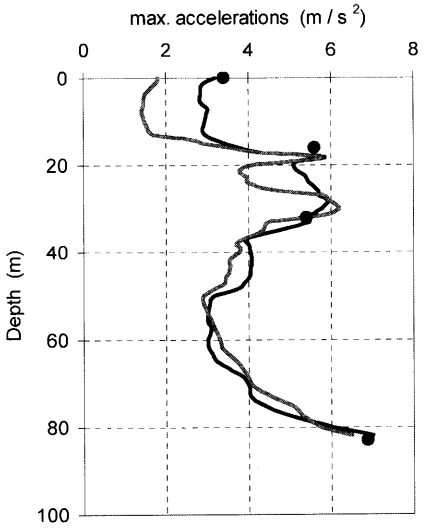

Fig. 26. Distribution of the maximum accelerations computed by the BWGG model (solid line) and the hyperbolic-plus-Masing model (gray line), together with the recorded values (circles)

response acceleration (after the 6 sec) is overestimated by the BWGG model. This is because no pore water pressure build-up was considered in the calibration of the model parameters.

Comparison between the spectral accelerations of the complete record at the ground surface and those computed by the BWGG model for the whole duration of motion is shown in Fig. 25. The agreement is satisfactory except for periods around 2 sec for which the response is overpredicted for the aforementioned reason. Figure 26 compares the distribution of maximum accelerations computed by the BWGG model and the hyperbolic-plus-Masing model, together with the recorded values. The agreement for the BWGG model is indeed good, and far better than that of the hyperbolic-plus-Masing model. The latter leads to a systematic cutting-off the acceleration time history at ground surface, even before the initiation of liquefaction (Fig. 22). This is mainly for the two aforementioned reasons: (a) the overestimation of the material damping at large strains, and (b) the zero post-yield hardening characterizing the model. These weaknesses of the hyperbolic-plus-Masing model in simulating cyclic behaviour, are shown in the stress-strain loops, at depths of 20 m and 32 m respectively, plotted in Fig. 23. The inability of the hyperbolic-plus-Masing model to capture the actual response is also evident in Figs. 24 and 25 where the computed spectral accelerations for periods between 1 and 3 seconds, are about two times lower than the recorded.

CONCLUSIONS

A phenomenological constitutive model, BWGG, is developed in this article for static and dynamic response of soil elements. The model is incorporated into a novel algorithm named NL-DYAS for the nonlinear inelastic one-dimensional ground response analysis of layered sites. It is shown that the model is very versatile in representing complex nonlinear characteristics of the cyclic behaviour of soil elements, such as stiffness decay with strain amplitude, loss of strength due to pore-water pressure development, cyclic mobility, and non-symmetric behaviour with loading direction. The proposed model has the ability to independently match experimental shear modulus and damping curves, by properly adjusting only three of its parameters. The NL-DYAS code was utilized to simulate the cyclic behaviour of a layered site subjected to seismic excitation. The results are compared with predictions of widely available and extensively used methods of analysis, such as the equivalent-linear and the hyperbolic nonlinear model. The comparison reveals the weakness of the aforementioned methods of analysis to simulate realistically the nonlinear cyclic behaviour of a soil deposit, at large strain levels. To provide some verification of the model, the records of the Port Island array during the Kobe 1995 earthquake were utilized. The model was shown to "predict" the observed response with sufficient accuracy. The hyperbolic model in conjunction with the Masing rules for unloading-reloading was also used for soil amplification analysis but was shown to be less successful in reproducing the reality.

REFERENCES

1) Bouc, R. (1971): Modele mathematique d' hysteresis, *Acustica*, **21**, 16–25.
2) Elgamal, A. W., Zeghal, M. and Parra, E. (1995): Identification and modeling of earthquake ground response, *Proc. 1st Int. Conf. Earthquake Geotech. Engrg.*, Tokyo, **3**, 1369–1406.
3) Finn, W. D. L., Lee, K. W. and Martin, G. R. (1977): An effective stress model for liquefaction, *J. Geotech. Engrg. Div.*, ASCE, **103** (6), 517–533.
4) Gerolymos, N. (2002): Constitutive model for static and dynamic response of soil, soil-pile, and soil-caisson, *PhD. Dissertation*, National Technical University, Athens (in Greek).
5) Gerolymos, N. and Gazetas, G. (2003): One-dimensional constitutive model for cyclic soil behavior applied to seismic analysis of multi-layered deposit, *Proc. Int. Workshop on Prediction and Simulation Methods in Geomechanics, IWS-Athens 2003*, 25–28.
6) Ishihara, K. and Towhata, I. (1980): One-dimensional soil response analysis during earthquakes based on effective stress model, *J. Faculty of Engineering, University of Tokyo*, **35** (4).
7) Iwasaki, Y. (1995): Geological and geotechnical characteristics of Kobe area and strong ground motion records by 1995 Kobe Earthquake, *Soils and Foundations, Special Issue on Geotechnical Aspects of the January 17, 1995 Hyogoken-Nambu Earthquake*, **43** (6), 15–20.
8) Kokusho, T. and Matsumoto, M. (1998): Nonlinearity in site amplification and soil properties during the 1995 Hyogoken-Nambu Earthquake, *Soils and Foundations, Special Issue on Geotechnical Aspects of the January 17, 1995 Hyogoken-Nambu Earthquake*, **38** (2), 1–9.
9) Kokusho, T., Sato, K. and Matsumoto, M. (1996): Nonlinear dynamic soil properties back-calculated from strong motions during Hyogoken-Nambu Earthquake, *Proc. 11th WCEE*, Acapulco.
10) Law, K. T., Cao, Y. L. and He, G. N. (1990): An energy approach for assessing seismic liquefaction potential, *Can. Geotech. J.*, **27** (3), 320–329.
11) Lee, M. K. W. and Finn, W. D. L. (1978): DESRA-2, Dynamic effective stress response analysis of soil deposits with energy trans-

mitting boundary including assessment of liquefaction potential, *Soil Mechanics*, 38, University of British Columbia, Vancouver.
12) Loh, C. H., Cheng, C. R. and Wen, Y. K. (1995): Probabilistic evaluation of liquefaction potential under earthquake loading, *Soil Dynamics and Earthquake Engineering*, **14**, 269–278.
13) Lok, T. M. H. and Pestana, J. M. (2000): An enhanced hysteretic model for site response analysis, *12th World Conf. on Earthquake Engineering*, New Zealand.
14) Pires, J. A., Ang, A. H-S. and Katayama, I. (1989): Probabilistic analysis of liquefaction, *Proc. 4th Int. Conf. Soil Dynamic and Earthquake Engineering*, Mexico.
15) Schnabel, P. G., Lysmer, J. and Seed, H. B. (1972): SHAKE, A computer program for earthquake response analysis of horizontally layered sites, *Report EERC 72-12, Earthquake Engineering Research Center*, University of California, Berkeley.
16) Sues, R. H., Mau, S. T. and Wen, Y.-K. (1988): Systems identification of degrading hysteretic restoring forces, *J. Engrg. Mech.*, ASCE, **114** (5), 833–846.
17) Travasarou, Th. and Gazetas, G. (2003): On the linear seismic response of soils with modulus varying as power of depth—the Maliakos marine clay, *Soils and Foundations*, **44** (5), 85–93.
18) Vucetic, M. and Dobry, R. (1989): Effect of soil plasticity on cyclic response, *J. Geotech. Engrg.*, ASCE, **117**, 89–107.
19) Wen, Y.-K. (1976): Method for random vibration of hysteretic systems, *J. Engrg. Mech.*, ASCE, **102**, 249–263.
20) Yamazaki, F., Ansary, M. A. and Towhata, I. (1995): Application of a dynamic effective stress model at a reclaimed site during the Great Hanshin earthquake, 1995, *Proc. 1st Int. Conf. Earthquake Geotech. Engrg.*, Tokyo, **1**, 591–597.